DEVELOPMENT AND VALIDATION OF A CRYOGENIC HYDROGEN VAPOR DISPERSION MODEL WITH INTEGRATED RISK ASSESSMENT FRAMEWORK FOR ACCIDENT SCENARIOS IN HYDROGEN REFUELING INFRASTRUCTURE

Yi-Yang Liu, Zhi-Xiang Xing*, and Ye-Cheng Liu*

School of Safety Science and Engineering, Changzhou University, No. 21, Gehu mid-Rd., Wujin Dist., Changzhou, 213164, Jiangsu, China

[*] Corresponding author; Email: xingzhixiang@cczu.edu.cn, lyc@cczu.edu.cn.

With the widespread application of hydrogen energy as a clean energy source, its safety issues are increasingly being emphasized. Hydrogen leakage can lead to fires or explosions, posing a threat to public safety. Conducting safety research on the diffusion patterns of liquid hydrogen leakage in response to this safety issue can help prevent and reduce hydrogen leakage accidents and protect people's lives and property. This study employs the computational fluid dynamics (CFD) software Fluent, in combination with the Lee model and the VOF model, to simulate the leakage and vaporization process of liquid hydrogen. It is found that an increase in wind speed extends the downwind diffusion distance and reduces the vertical height. Based on the diffusion patterns of the combustible gas cloud and in view of the limitations of hydrogen sensors, a new method of using temperature sensors to monitor environmental temperature changes to predict hydrogen concentration is proposed. By analyzing the mathematical relationship between temperature and hydrogen concentration during the initial stage of leakage, a mathematical model is established. The validation of the model shows that temperature sensors arranged on the 0.8 m height plane can quickly respond to leakage events, thereby enhancing the safety management level of hydrogen refueling stations.

Key words: liquid hydrogen leakage, numerical simulation, flammable gas cloud dispersion, hydrogen refueling station safety, hydrogen concentration prediction

1. Introduction

The increasing energy demand and environmental concerns are prompting a shift in energy sources, with hydrogen emerging as a zero-emission, high-calorific-value alternative for sustainable automotive fuels. However, hydrogen poses safety risks due to its high leak tendency, low ignition energy (0.02 mJ), and wide explosive range (combustion: 4%–75%; explosion: 18.3%–59%). Compared to fossil fuels, hydrogen is more hazardous, making the prevention and prompt response to hydrogen leaks critical for safety.

Hydrogen energy is mainly used in urban areas for new energy vehicles, with hydrogen refueling at stations being prone to leaks. Safe hydrogen application requires pressurized or cryogenic storage methods. Liquid hydrogen has higher energy density but poses significant safety risks, necessitating leak prevention and protective measures. Hydrogen release accidents occur at higher rates compared to other substances, with releases classified into enclosed, semi-enclosed, and open environments. At refueling stations, liquid hydrogen tanks are typically in semi-enclosed settings with fire barriers. Risk assessment involves hydrogen leakage and local environmental factors such as leak point characteristics, wind effects, and atmospheric visibility. Numerous studies have been conducted on hydrogen leakage and diffusion mechanisms. To predict cryogenic liquid danger zones for accidental leakage, extensive experiments have been performed to calculate the leakage and diffusion characteristics of flammable and cold effect clouds. NASA [1–2], BAM [3], and HSL [4] have conducted experimental studies on liquid hydrogen, obtaining valuable data for predicting harmful effects. However, due to high cost and risk, experiments are limited, and computational fluid dynamics (CFD) has become the mainstream research method for liquid hydrogen leakage simulation. Various CFD software, such as ANSYS FLUENT, ANSYS CFX, FLACS [5–6], OPEN FOAM, and GASFLOW-MPI [7], can simulate substance flow and diffusion in the atmosphere [8]. Wang et al. [9] studied the effects of leakage diameter, roof configuration, and ignition location on hydrogen diffusion, combustion, and hazard analysis. Liang et al. [10] developed a mixed four-phase flow model for liquid hydrogen release based on HSL tests, studying near-field liquid phase motion, combustible cloud, and far-field cold effect cloud motion. Tang et al. [11] conducted CFD simulations of hydrogen leakage in tunnels, underground parking lots, and multi-storey parking lots due to fuel cell vehicle accidents. Giannissi et al. [12–15] simulated liquid pool formation and hydrogen diffusion using a two-phase (liquid-gas) jet model. Mao et al. [16] used ANSYS fluent to simulate hydrogen leakage and diffusion in hydrogen energy compartments, analyzing overpressure and high-temperature damage from explosions. Qian et al. [17,18] studied accidental hydrogen release under different states for risk analysis and consequence assessment of hydrogenation stations. Jiang et al. [17] designed a wireless sensor network layout based on meteorological and gas characteristics, conducting field tests in a chemical industry park. Marco et al. [19] developed a method for hazardous gas detector placement in complex industrial layouts. Sklavounos et al. [20] simulated large-scale leakage tests of liquefied hydrogen and natural gas, with concentration data matching experimental records. Dong et al. [21,22] optimized sensor layout in chemical parks through numerical simulations. Tanaka [23] et al. Shirvill [24] et al. Kobayashi [25] et al. conducted the experimental study on the hydrogen explosion risk of hydrogen refueling stations. Kim et al. [26] took a commercially operated hydrogen refueling station in South Korea as the research object to study the effects of hydrogen cylinder pressure and leak hole diameter on hydrogen leakage and explosion behavior. For large leaks, it is not appropriate to evaluate the hydrogen concentration distribution on a time average basis. It is necessary to grasp the instantaneous concentration distribution with a high response sensor. Idris et al. [27] proposed a risk-based approach to optimize the placement of combustible gas detectors by integrating the formula of fuzzy multi-objective mixed integer linear programming to minimize residual risks and the total number of detectors, so as to achieve effective explosion protection. Zhang et al. [28] reviewed and analyzed the principle, applicability and research status of different types of hydrogen sensors, and prospected their development trend. Gao et al. [29] calculated the amount of hydrogen leakage based on the leakage model for the scenario of hydrogen leakage in the cabin. Then, Fluent software was used to simulate the diffusion process of hydrogen between the two vehicles, and the change rule of hydrogen concentration was obtained. Finally, the influence factors of hydrogen diffusion distribution in the cabin are analyzed by simulation under different leakage locations and ventilation conditions. The simulation results determine the optimal position of the hydrogen sensor.

In the hydrogen refueling station, the area of the liquid hydrogen storage tank is most prone to leakage. Few studies have focused on the rapid detection of flammable gas clouds under the same working conditions but different wind speeds using different common sensors. Pu et al. [30] have made a breakthrough in this field by innovatively constructing a hybrid model of multi-component phase change flow that integrates the phase change process of liquid hydrogen. The model has been tested and verified by the authoritative Health and Safety Laboratory (HSL) in the UK, providing a reliable theoretical basis for subsequent research on leakage detection. Therefore, this paper will model and analyze the diffusion behavior and safety of liquid hydrogen leakage from the storage tank in the hydrogen refueling station under different wind speeds and directions, and propose a method to improve the efficiency of hydrogen leakage detection by the synergistic action of temperature sensors.

2. Liquid hydrogen leakage endothermic gasification model

The leakage of liquid hydrogen involves rapid phase changes due to the significant temperature difference between the liquid hydrogen and the environment. Given the low boiling point (20.32 K) and storage temperature (20 K), minimal heat absorption causes liquid hydrogen to vaporize. The Lee model, effectively simulates these phase changes by describing evaporation and condensation processes. It can be coupled with the VOF multiphase flow model or the Eulerian multiphase flow model using an overall interface heat transfer coefficient. In this study, the Lee model and VOF multiphase flow model are employed to simulate the phase change from liquid to gaseous hydrogen, with the evaporation mass transfer process governed by the vapor transport Equation.

$$\frac{\partial}{\partial t}(\alpha_v \rho_v) + \nabla \cdot \left(\alpha_v \rho_v \vec{V}_v\right) = \dot{m}_{lv} - \dot{m}_{vl} \tag{1}$$

Where v represents the gas phase, α_v is the volume fraction of hydrogen vapor, ρ_v is the density of hydrogen vapor, $\vec{\boldsymbol{V}}_v$ is the velocity of the hydrogen gas phase, $\dot{m}_{lv}$ is the mass transfer rate caused by evaporation, and $\dot{m}_{vl}$ is the mass transfer rate caused by condensation, with the unit of kg*(s*m^3)$^{-1}$.

For the following temperature conditions, mass transfer can be described as follows:

If the condition $T_l > T_{sat}$ (evaporation case) arises.

$$\dot{m}_{lv} = coeff \cdot \alpha_l \rho_l \frac{(T_l - T_{sat})}{T_{sat}} \tag{2}$$

If the condition $T_v < T_{sat}$ (condensation case) arises

$$\dot{m}_{vl} = coeff \cdot \alpha_v \rho_v \frac{(T_{sat} - T_v)}{T_{sat}} \tag{3}$$

Where $'coeff'$ is an adjustable coefficient, which can be interpreted as a relaxation coefficient. 'α' and 'ρ' represent the volume fraction and density of the phase, respectively. 'T' stands for temperature, with 'l' and 'v' denoting the liquid and vapor phases, respectively, and 'sat' refers to the saturation value.

Through simulations with multiple sets of phase change coefficients, the evaporation and condensation frequencies are set to 0.06 and 0.50, respectively, with the saturation temperature in the hydrogen phase interaction being 20.32 K.

3. Model building and simulation

3.1 The establishment of mathematical model

The leak diffusion model is conducted using the CFD simulation software Fluent. The CFD simulation adopts a three-dimensional transient finite volume method, which has been applied in the simulation of various substance diffusion and leakage problems, and its accuracy has been affirmed. In the case of liquid hydrogen evaporation in this paper, the Eulerian phase number is set to 2, with the primary phase being air and the secondary phases being hydrogen gas and liquid hydrogen. There are two types of gases in this simulation, both of which are incompressible ideal gases because the Mach number of the flow within the domain is much less than 0.3. For turbulence, the $k-\varepsilon$ atmospheric turbulence model with enhanced wall treatment and mixed drift force is used in this simulation.

The continuity equation is:

$$\frac{\partial}{\partial t}(\rho_m) + \nabla(\rho_m \overrightarrow{v_m}) = 0 \tag{4}$$

In this context, ρ_m represents the mixture density, and $\overrightarrow{\boldsymbol{v_m}}$ represents the mass-average velocity.

The momentum equation can be obtained by summing the individual momentum equations of all phases. It can be expressed as:

$$\frac{\partial}{\partial t}(\rho_m \vec{v}_m) + \nabla \cdot (\rho_m \vec{v}_m \vec{v}_m) = -\nabla p + \nabla \cdot [\mu_m(\nabla \vec{v}_m + \nabla \vec{v}_m^T)] + \rho_m \vec{g} + \vec{F} - \nabla \cdot \left(\sum_{k=1}^{n} \alpha_k \rho_k \vec{v}_{dr,k} \vec{v}_{dr,k}\right) \tag{5}$$

Where p is the pressure, the viscosity of the flavor mixture μ_m, n is the number of phases, and the value in this simulation is 2, $\vec{g}$ the acceleration of the object acting on the flavor on the continuity, such as gravity, inertial force, etc. $\vec{F}$ volume force, α_k is the volume fraction of the air phase, $\vec{v}_{dr,k} = \vec{v}_k - \vec{v}_m$ is the drift velocity of the secondary phase k.

Energy equation can be shown as following:

$$\frac{\partial}{\partial t}\sum_{k=1}^{n}(\alpha_k \rho_k E_k) + \nabla \cdot \sum_{k=1}^{n}[\alpha_k \vec{v}_k(\rho_k E_k + p)] = \nabla \cdot (k_{eff} \nabla T) \tag{6}$$

In the formula, k_{eff} represents the effective thermal conductivity, and $\vec{\boldsymbol{v}}_{\boldsymbol{k}}$ is the velocity of phase k. For an incompressible fluid, E_k is the standard enthalpy of phase k.

3.2 The definition of computational domain and boundary conditions

3.2.1 Model setup

According to the relevant provisions of the "Hydrogen Refueling Station Design Code" GB50177–2021, a model is established for the hydrogen refueling station. The hydrogen refueling station scenario is defined as a finite space where liquid hydrogen can move freely with complex obstacles. Due to the complexity of the wind field, the length of the computational domain is set to 121 meters, the width to 91 meters, and the height to 30 meters, as shown in Fig. 1. This is sufficiently large for the study of liquid movement, gas evaporation diffusion, and the impact of wind fields on flammable gas clouds. The front side (YZ plane, x=0 m), left side (XZ plane, y=0 m), right side (XZ plane, y=121 m), and the top side (XY plane, z=30 m) are all set as pressure outlets. The liquid hydrogen leakage port is set as a mass flow rate inlet, located at the connection between the liquid hydrogen storage tank and the pipeline (centered on the point (93.500, 55.125, 1.406) with a radius of R=24.4m in the XZ plane, and the leakage direction is parallel to the XY plane, with the liquid hydrogen leakage direction towards the positive X-axis. The back side (YZ plane, x=121 m) is set as a natural atmospheric velocity inlet. The bottom (XY plane, z=0 m) is set as an immovable stationary wall.

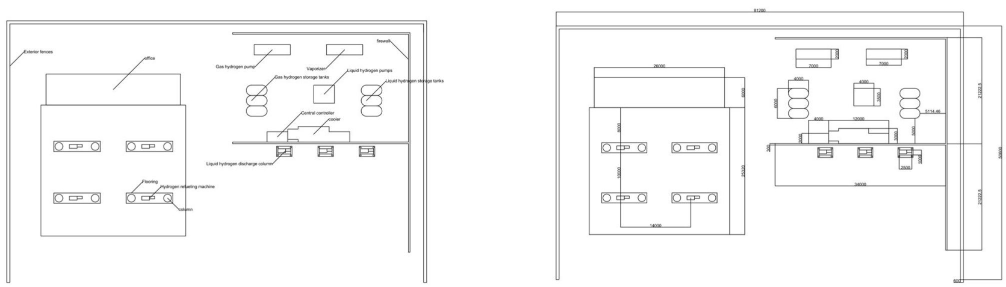

（a）　　　　　　　　　　　　（b）

Figure 1. Geometric structure model of hydrogen refueling station:(a) Functional layout of hydrogen refueling station;(b) Detailed dimensional drawing of hydrogen refueling station.

3.2.2 Boundary condition setting and mesh independence verification

The model operating conditions and parameter settings are as follows. The maximum liquid hydrogen storage capacity of the liquid hydrogen storage tank in the hydrogen refueling station under full load is assumed to be 2.22 t. According to the "Liquid Hydrogen Storage Process and Facilities" (GB50156-2021), the working pressure range of the inner container of the liquid hydrogen storage tank is 0.10 MPa to 0.98 MPa, with an intermediate value of 0.54 MPa used in this study. A leakage port with a diameter of 48.8 mm is located at the liquid hydrogen pipeline connection for the leakage simulation. The leakage rate is directly proportional to the area of the leakage port, based on fluid mechanics principles. The specific formula is as follows:

$$\dot{m} = C_d A\sqrt{2\rho(P - P_{\mathrm{atm}})} \quad (7)$$

In the formula, $\dot{m}$ represents the leakage rate (in units of kg/s); C_d is the discharge coefficient; A is the area of the leakage opening (in units of m²); ρ is the density of liquid hydrogen (in units of kg/m³); P is the pressure inside the storage tank (in units of Pa); P_{atm} is the atmospheric pressure (in units of Pa).

The mass flow leakage rate is calculated to be 9.52 kg/s according to Equation (7). To study the impact of environmental factors on the diffusion of flammable hydrogen gas clouds, three categories of wind speeds are simulated: low (1 m/s and 3 m/s), medium (5 m/s), and high (7 m/s and 9 m/s). The environmental temperature and atmospheric pressure are set at 300 K and 101,325 Pa, respectively. The saturation temperature of liquid hydrogen is 20.32 K, and in storage, it is in a subcooled state at 19.58 K.

The Fluent solution method has been validated through experiments conducted by the Health and Safety Laboratory. The research by Giannissi, S. G. et al. [12-15] also demonstrated that Fluent computational fluid dynamics is realistic and effective for simulating liquid hydrogen leakage. The hydrogen refueling station model uses a hexahedral core mesh with refined meshing around the leakage source and coarser meshing in the far-field flow region. The mesh distributions are shown in Fig. 2a, b, and c. Four mesh counts were tested: 19,495,652, 2,666,206, 1,377,923, and 597,034. The average volume fraction of liquid hydrogen within the diffusion zone over time was used as the mesh differentiation indicator, with results shown in Fig. 2d. As the mesh count increased, the average volume fraction stabilized, with no significant difference between 2,666,206 and 19,495,652. Therefore, a mesh count of 2,666,206 was selected for subsequent studies. Tests confirmed that this mesh count did not affect the simulation results. The solution parameter settings for the simulation are shown in Table 1.

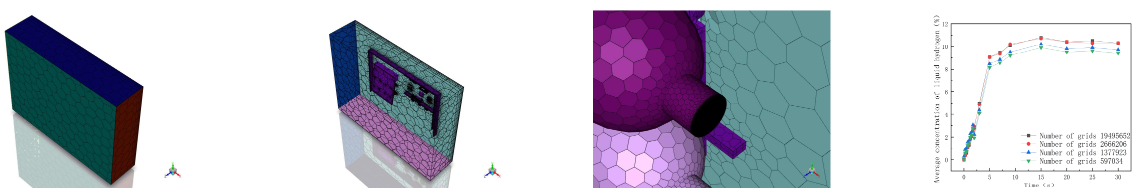

(a) (b) (c) (d)

Figure 2. Mesh Independence Verification: (a) Appearance of the global mesh; (b) Internal condition of the global mesh; (c) Local mesh near the leakage port; (d) Mesh independence testing.

Table 1-Solution method of liquid hydrogen leakage simulation.

Parameters	Solution methods
Pressure-velocity coupling	PISO scheme
Gradient spatial discretization	Least Squares Cell Based
Pressure spatial discretization	Body Force Weighted
Other parameters spatial discretization	QUICK
Transient formulation	Second order implicit
Convergence criterion	10-6 in steady cases, 10-6 in transient cases
Step size	0.005s

4. Result analysis and discussion

4.1 Study on liquid hydrogen leakage phase transition process and gasification law

In this study, liquid hydrogen leakage is simulated at the connection between the storage tank and pipeline, centered at (93.500, 55.143, 1.406) with a 24.40mm radius on the XZ plane. During leakage, the cold liquid hydrogen exchanges heat with the warmer environment, absorbing heat from air and nearby surfaces. Given the low vaporization temperature of liquid hydrogen (20.32 K) compared to its storage temperature (19.58 K), a rapid phase change occurs. Since hydrogen is flammable at air volume fractions between 4% and 75%, the resulting hydrogen gas can readily form flammable clouds. The diffusion patterns, shown in Fig. 3 and Fig. 4, can be divided into four stages.

Initially, during the free outflow phase as depicted in (Fig. 3a and Fig. 4a), a small amount of liquid hydrogen leaks out at the beginning (0-1.5 seconds). It exchanges heat with the environment, generating hydrogen gas and causing a decrease in ambient temperature. The combustible hydrogen gas cloud is small in volume and descends. Subsequently, in the phase change and sedimentation phase shown in (Fig. 3b and Fig. 4b), after free outflow (5-15 seconds), the leakage volume increases, producing a large amount of low-temperature combustible hydrogen gas. The ambient wind fails to effectively dilute the hydrogen gas, leading to the accumulation of high-density hydrogen gas above the liquid hydrogen, exhibiting the diffusion characteristics of heavy gas. Then, in the ascending diffusion phase as illustrated in (Fig. 3c and Fig. 4c), as the leakage continues (30-40 seconds), the hydrogen gas concentration decreases and the diffusion rate slows down, but the vertical diffusion is enhanced. The hydrogen gas cloud transitions from heavy gas to light gas diffusion, moving upwards. Finally, in the stable diffusion phase shown in (Fig. 3d and Fig. 4d), from the end of the leakage to the end of the simulation, the flow field parameters stabilize, with small fluctuations in safety indicators such as temperature, concentration, and density. Due to the continuous leakage, the earlier phases also continue to occur, but the overall diffusion trend of the combustible gas cloud presents the characteristics of the later phases.

In the present study, the stable state of the combustible gas cloud depicted in Fig. 3c and Fig. 3d exhibits a high degree of consistency with the shape and concentration distribution of the combustible hydrogen gas cloud observed in the liquid hydrogen leakage experiment conducted by the National Aeronautics and Space Administration (NASA) in 1980 [2–3]. This finding not only substantiates the precision of the model employed in this research but also lays a reliable foundation for the model, thereby ensuring the scientific validity and credibility of the research outcomes.

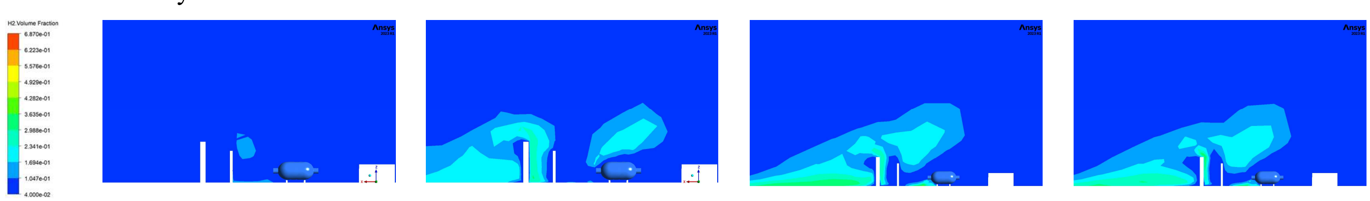

(a) (b) (c) (d)

Figure 3. Hydrogen diffusion process: (a) Hydrogen diffusion state at 0.75s; (b) Hydrogen diffusion state at 8.5s; (c) Hydrogen diffusion state at 37.5s; (d) Hydrogen diffusion state at 60.0s

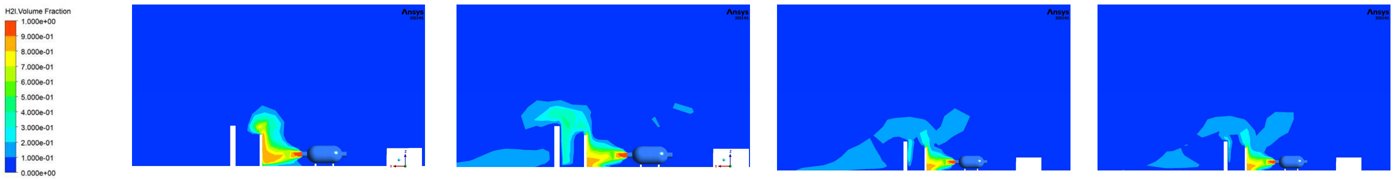

(a) (b) (c) (d)

Figure 4. Liquid hydrogen diffusion process: (a) Liquid hydrogen diffusion state at 0.75s; (b) Liquid hydrogen diffusion at 8.5s; (c) Liquid hydrogen diffusion state at 37.5s; (d) Liquid hydrogen diffusion state at 60s.

The maximum displacement and three-dimensional size of the flammable combustible gas cloud, with a wind speed of 5 m/s, are depicted in Fig. 5. In the downwind direction (X-axis), the flammable combustible gas cloud is initially driven by the liquid hydrogen outflow momentum during the natural outflow phase, resulting in rapid movement and diffusion. As phase change hydrogen increases, diffusion stabilizes, reaching a maximum downwind distance of 63.42 meters under stable environmental wind conditions. In the Y-axis direction (perpendicular to the wind), the cloud's diffusion is driven by the hydrogen gas momentum, achieving a maximum distance of 45.64 meters, with a diffusion pattern similar to that in the X-axis direction. Vertically, the flammable combustible gas cloud initially exhibits heavy gas diffusion characteristics, moving in low-altitude areas due to gravity. As the density difference between the combustible gas cloud and air becomes significant, buoyancy drives upward diffusion, with the maximum height varying with different wind speeds.

Obstacles significantly affect the diffusion behavior of hydrogen gas by altering the flow path of ambient wind. The simulation results show that when encountering obstacles, the wind speed decreases on the windward side (e.g., a reduction of about 40% under the 5 m/s condition) and forms a local recirculation zone behind the obstacle. Meanwhile, the geometric features of the obstacle edges induce an increase in turbulence intensity (with an increase of 22.13% in turbulent kinetic energy), accelerating the mixing of hydrogen gas with air. However, this can also lead to temporary accumulation of hydrogen gas clouds in the vortex region (Fig. 6a and 6b). The presence of a firewall forces the airflow to bypass, creating a diffusion divergence in the Y-axis direction, resulting in an increase of 27.81% in the lateral diffusion distance compared to the condition without obstacles (Fig. 6b). The blocking effect of obstacles significantly changes the diffusion path of hydrogen gas. In semi-enclosed areas such as tanks and firewalls, hydrogen gas clouds accumulate on the windward side due to restricted diffusion, with the maximum volume fraction increasing by 32.74% compared to open areas (Fig. 7a). Moreover, under complex obstacle layouts, hydrogen gas clouds diffuse along multiple branches (e.g., divergence in the X-axis and Y-axis directions). Under the 5 m/s wind speed condition, obstacles shorten the downwind diffusion distance by 19.86% but expand the lateral diffusion range to 45.64 m (Fig. 6b).

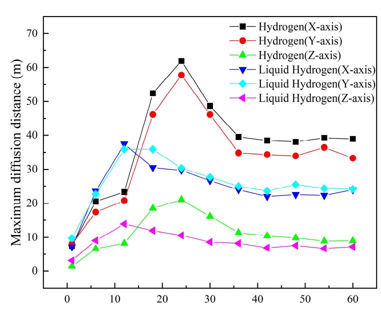

Figure 5. Variation of diffusion distance with time

4.2 Effect of wind speed on diffusion of combustible gas clouds

As shown in Fig. 6, the concentration distribution of flammable combustible gas clouds under different wind speeds (1–9 m/s) during liquid hydrogen leakage is presented. The diffusion trend is consistent, with the cloud moving towards the front of the hydrogen refueling station. With increasing wind speed, the cloud's X-axis length decreases (from 65.35 m at 1 m/s to 15.74 m at 9 m/s), while its Y-axis length increases (from 14.97 m to 42.55 m). The environmental wind drives long-distance diffusion along the wind direction, reducing natural convection and initial momentum effects. Higher wind speeds enhance hydrogen-air mixing, decreasing the cloud's volume fraction and height (from 14.73 m to 4.24 m along the Z-axis).

(a) (b)

Figure 6. Diffusion distances of hydrogen/liquid hydrogen at different wind speeds: (a)Maximum moving distance of liquid hydrogen gas at different wind speeds;(b)Maximum moving distance of liquid hydrogen at different wind speeds.

4.3 Relationship between gas cloud concentration and temperature

Consider the calculation and the composition of all gases in it as ideal gases, according to the ideal gas equation:

$$PV = nRT \tag{8}$$

In this context, P represents the pressure of the gas (unit Pa); V represents the volume of the gas (unit m^3); n represents the number of moles of the gas (unit mol); R is the ideal gas constant, with a value of 8.31; T represents the absolute temperature of the gas (unit K).

An inverse relationship between hydrogen concentration and temperature can be established, which can be used to calculate the corresponding hydrogen concentration based on the results of temperature measurements. Given the characteristics of hydrogen's low molecular weight, low density, and atmospheric disturbances, the hydrogen gas produced by the phase change of liquid hydrogen leakage in actual hydrogen refueling station scenarios is difficult to be captured by the hydrogen gas sensors above the leak source. Moreover, the hydrogen gas sensors currently available on the market generally suffer from delayed response, low response accuracy, and high cost, while high-precision sensors that can respond quickly to hydrogen flammable gases are still in the development and research stages in laboratories. Therefore, taking advantage of the rapid response and low cost of temperature sensors, the monitoring of the difference in environmental temperature, and the processing and calculation of the temperature signal can be used to measure the leakage concentration, thereby improving the level of hydrogen concentration detection in hydrogen refueling stations and making them safer.

When a leak begins, the temperature distribution and hydrogen concentration distribution within the Z=0.55m plane are shown in Fig. 7abc. It can be seen that the distribution of temperature is similar to that of hydrogen concentration, which means that the area with the lowest temperature coincides with the area of the highest concentration, consistent with the conclusion derived from the adiabatic mixing principle regarding the relationship between temperature and concentration. Based on this relationship, random points are taken within the Z=0.55m plane, as shown in Fig. 7d, it can be seen that there is a linear correlation between temperature and hydrogen concentration. Based on this linear correlation, a relationship formula between hydrogen concentration and temperature can be fitted as follows:

$$C = -0.000116794 * T + 0.03503 \tag{9}$$

Where C represents the volume fraction of hydrogen (unit vol%); T represents the ambient temperature (K).

As shown in Fig. 7e, there is an inverse proportional function correlation between liquid hydrogen concentration and temperature, the relationship can be approximated as an inverse proportion function, which can be fitted as:

$$C = 0.09163 * \exp\left(\frac{-T}{119.23766}\right) - 0.007491 \tag{10}$$

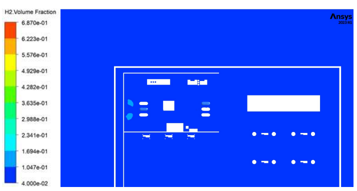

(a)

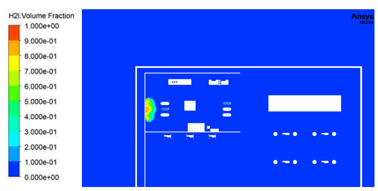

(b)

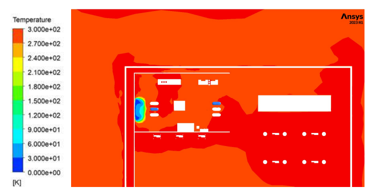

(c)

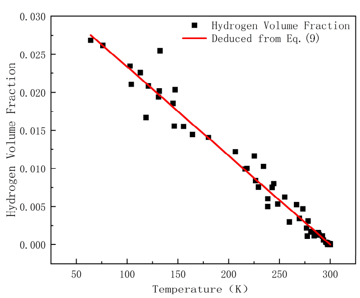

(d)

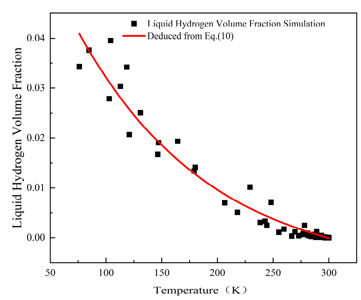

(e)

Figure 7. Relationship between temperature and liquid/gaseous hydrogen: (a) hydrogen volume fraction; (b) liquid hydrogen volume fraction; (c) temperature; (d) Hydrogen volume fraction/temperature fit; (e) Liquid Hydrogen volume fraction/temperature fit.

To verify the accuracy of Equation (9) and Equation (10) for detecting leaks in complex environments, their applicability at the start of leakage is assessed. According to GB/T50493-2019 , detectors for heavy gases should be installed at specific heights: 0.3m to 0.6m above the floor for gases heavier than air, and 0.5m to 1.0m below the release source for gases slightly heavier than air. Points are taken at 0.3m, 0.4m, 0.7m, and 0.8m heights to compare the calculated values of hydrogen and liquid hydrogen relationships (Fig. 8a and Fig. 8b) with simulated concentration values. Equation (9) shows a maximum relative error of 18.04% at 72.86K, while Equation (10) has a maximum relative error of 13.07% at 208.42K. Both errors are below 20%, and the calculated values are higher than the simulated values, which is acceptable for hydrogen refueling station safety. The relative errors of the two relational expressions are both less than 20%, and the calculated values are higher than the simulated values. In safety monitoring, the priority is to ensure the safety of the hydrogen refueling station. The higher calculated values mean that the system will tend to trigger alarms earlier or more frequently.

For example, when the actual concentration has not yet reached the dangerous threshold, the predicted value may already be close to or exceed the safety limit, prompting the safety measures to be activated in advance, thereby reducing the risk of false negatives and prioritizing the safety of personnel and facilities. Therefore, this error is acceptable. The smallest error and highest accuracy are observed on the 0.8m plane (Fig. 8c and Fig. 8d), suggesting that temperature sensors should be placed there for rapid leak detection. The error in predicted concentration values is related to the phase change of liquid hydrogen, which absorbs heat during evaporation.

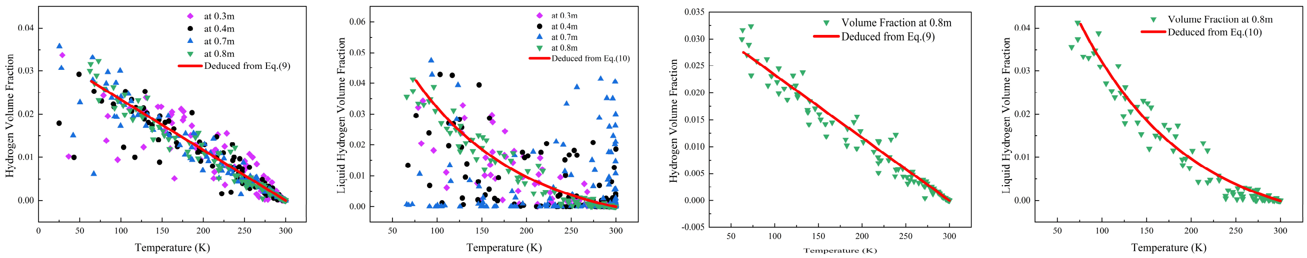

(a) (b) (c) (d)

Figure 8. Comparison and verification of the gas-liquid two-phase fitting relationship with the simulated value:(a) Comparison of simulated hydrogen gas values at different heights and fitting values of Eq.9;(b) Comparison of simulated values of liquid hydrogen at different heights and fitting values of Eq.10;(c)z=0.8m The simulated value of hydrogen is compared with the fitting value of Eq.9;(d) The simulated value of liquid hydrogen is compared with the fitting value of Eq.10.

4.4 Temperature sensor layout point selection

Based on the conclusions drawn in the previous section, an analysis of the layout of temperature sensors on the 0.8m plane is conducted. According to the relevant regulations in the national standards, when the release source is located in an enclosed workshop or a semi-open workshop with poor local ventilation, the horizontal distance between the flammable gas detector and any release source within its coverage should not exceed 5 meters. As shown in Fig. 9a, taking an environmental wind speed of 5m/s as an example, the environmental wind encounters a reduction in wind speed when it meets the complex obstacles inside the hydrogen refueling station, and the surrounding of the hydrogen production and storage station is equipped with walls or fire walls, so the hydrogen storage area of the refueling station can be regarded as a semi-open workshop with poor local ventilation. Therefore, this point can be adopted when setting up temperature sensors. In this section, temperature sensors are arranged within a circle centered on the leak source with a radius of 5m to verify their detection effect [19]. The positions of the temperature sensors are shown in Fig. 9b, representing the installation locations of temperature sensors in different directions as shown in Table 2.

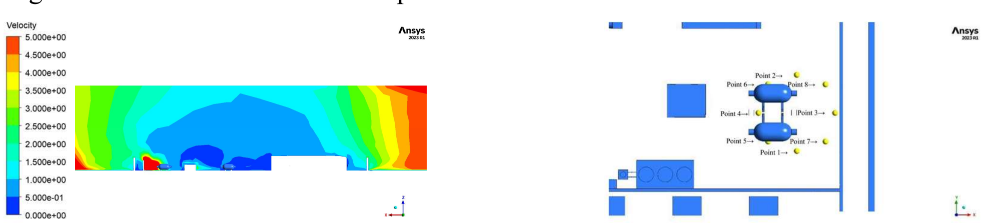

（a） （b）

Figure 9. Location selection of temperature sensor： (a) Wind speed distribution at 5m/s; (b) Temperature sensor distribution.

Table 2-Sensor position distribution table.

Serial number	X-axis coordinate	Y-axis coordinate	Z-axis coordinate
Point #1	72.5m	31.125m	0.8m
Point #2	72.5m	39.125m	0.8m
Point #3	76.5m	35.125m	0.8m
Point #4	68.5m	35.125m	0.8m
Point #5	69.5m	32.125m	0.8m
Point #6	69.5m	38.125m	0.8m
Point #7	75.5m	32.125m	0.8m
Point #8	75.5m	38.125m	0.8m

In the given context, sensors 3, 7, and 8 were the first to detect temperature changes at 0.5 seconds. Sensor 7 demonstrated a high degree of consistency between its calculated concentration and the actual simulated concentration. This indicates that placing temperature sensors on the downwind side of the environmental wind can lead to an early and accurate detection of the concentration at the onset of a leak. Without altering any other conditions, the environmental wind direction was changed from parallel to the leak direction to perpendicular, and the response speed of the sensors was further verified. As shown in Table 3, changing the wind direction did not alter the initial data captured by the sensors. Consistently, sensor 7 was the first to detect the temperature change, which corresponded to the simulated concentration values with the smallest margin of error. From this, it can be concluded that positioning temperature sensors at this location (3 meters from the leak direction and 3 meters downwind) can accurately assist in addressing the issue of delayed alarms caused by the slow response of hydrogen gas sensors, thereby enhancing the capability for precise and timely warning of leaks.

Table 3-Point #7 Liquid hydrogen/gas hydrogen calculated values compared with simulated values.

Working condition Wind speed	Eq.(9) Calculated concentration	Hydrogen simulated concentration	Relative error	Eq.(10) Calculated concentration	Liquid hydrogen simulation concentration	Relative error
1m/s	3.146%	2.972%	5.85%	6.347%	6.121%	3.58%
3m/s	3.132%	3.172%	1.26%	6.271%	7.007%	6.22%
5m/s	3.088%	2.841%	8.73%	6.052%	6.338%	4.51%
7m/s	3.084%	3.337%	7.58%	6.031%	5.685%	6.09%
9m/s	3.052%	2.943%	3.81%	5.877%	5.535%	6.18%

5. Conclusion

This study establishes a validated CFD framework for simulating liquid hydrogen leakage and dispersion, offering critical insights into risk assessment for hydrogen refueling stations. Key findings include:

（1） By employing the Lee model and the VOF multiphase flow model in combination with the CFD simulation software Fluent, the phase change process and vaporization pattern of liquid hydrogen leaking into the environment can be effectively simulated. The simulation results indicate that after liquid hydrogen leakage, it rapidly exchanges heat with the surrounding environment, forming a combustible gas cloud, a process that is significantly influenced by ambient wind speed.

（2） The diffusion process of the combustible gas cloud generated by liquid hydrogen leakage can be divided into four stages: free outflow, phase change and sedimentation, upward diffusion, and diffusion stabilization. An increase in wind speed affects the diffusion of the combustible gas cloud in both horizontal and vertical directions, resulting in an increased downwind diffusion distance and a reduced maximum height in the vertical direction.

（3）Due to the response hysteresis and high cost of hydrogen sensors, monitoring environmental temperature changes using temperature sensors becomes an economically effective alternative. By analyzing the linear relationship between temperature and hydrogen concentration, the distribution of hydrogen concentration can be accurately predicted. Temperature sensors arranged on a specific height plane can quickly respond to leakage events, thereby enhancing the safety management level of hydrogen refueling stations.

（4）The study has determined the optimal placement of temperature sensors around the leakage source to achieve accurate early warning of liquid hydrogen leakage. Temperature sensors arranged on the 0.8 m height plane can quickly respond to leakage events, thereby enhancing the safety management level of hydrogen refueling stations.

These results demonstrate the model's capability to guide safety enhancements, such as optimized sensor layouts and barrier configurations, directly applicable to hydrogen refueling station design and emergency protocols. Future work will integrate real-time data assimilation to further refine predictive accuracy.

Acknowledgements

This work was supported by the National Key Research and Development Plan (No.2022YFB4002803) and the Innovation Capacity Building Plan for Technology Infrastructure (No. BM2022013).

References

[1] LI, J. F., *et al*., Diffusion features of jet leakage with liquid hydrogen in large space, *CIESC Journal*, 73 (2022), 11, 5177–5185.

[2] Witcofski, R. D., Chirivella, J. E., Experimental and analytical analyses of the mechanisms governing the dispersion of flammable clouds formed by liquid hydrogen spills, *International Journal of Hydrogen Energy*, 9 (1984), 5, 425–435.

[3] Statharas, J. C., *et al*., Analysis of data from spilling experiments performed with liquid hydrogen, *Journal of Hazardous Materials*, 77 (2000), 1-3, 57–75.

[4] Hooker P, *et al*. Experimental releases of liquid hydrogen[C]. *International Conference on Hydrogen Safety*, (2011).

[5] Xiao, J. S., *et al*., Computational fluid dynamics model based artificial neural network prediction of flammable vapor clouds formed by liquid hydrogen releases, *International Journal of Energy Research*, 46 (2022), 8, 11011–11026.

[6] Zhou, C. L., *et al*., Optimizing hydrogen refueling station layout based on consequences of leakage and explosion accidents, *International Journal of Hydrogen Energy*, 54 (2024), 817–836.

[7] Xiao, J. J., *et al*., GASFLOW-MPI: A new 3-D parallel all-speed CFD code for turbulent dispersion and combustion simulations: Part I: Models, verification and validation, *International Journal of Hydrogen Energy*, 42 (2017), 12, 8346–8368.

[8] Middha, P., Hansen, O. R., Using computational fluid dynamics as a tool for hydrogen safety studies, *Journal of Loss Prevention in the Process Industries*, 22 (2009), 3, 295–302.

[9] Wang, F. N., *et al*., Deterministic risk assessment of hydrogen leak from a fuel cell truck in a real-scale hydrogen refueling station, *International Journal of Hydrogen Energy*, 50 (2024), 1103–1118.

[10] Pu, L., *et al*., Plume dispersion behaviour and hazard identification for large quantities of liquid hydrogen leakage, *Asia-Pacific Journal of Chemical Engineering*, 14 (2019), 2, e2299.

[11] Tang, X., *et al*., Dispersion behavior and safety study of liquid hydrogen leakage under different application situations, *International Journal of Hydrogen Energy*, 45 (2020), 55, 31278–31288.

[12] Giannissi, S. G., Venetsanos, A. G., A comparative CFD assessment study of cryogenic hydrogen and LNG dispersion, *International Journal of Hydrogen Energy*, 44 (2019), 17, 9018–9030.

[13] Giannissi, S. G., Venetsanos, A. G., Study of key parameters in modeling liquid hydrogen release and dispersion in open environment, *International Journal of Hydrogen Energy*, 43 (2018), 1, 455–467.

[14] Giannissi, S. G., *et al*., On the CFD modelling of hydrogen dispersion at low-Reynolds number release in closed facility, *International Journal of Hydrogen Energy*, 46 (2021), 57, 29745–29761.

[15] Giannissi, S. G., *et al*., CFD modeling of hydrogen dispersion under cryogenic release conditions, *International Journal of Hydrogen Energy*, 39 (2014), 28, 15851–15863.

[16] Mao, X. B., *et al*., Simulation and analysis of hydrogen leakage and explosion behaviors in various compartments on a hydrogen fuel cell ship, *International Journal of Hydrogen Energy*, 46 (2021), 9, 6857–6872.

[17] Jiang, Y., *et al*., Optimized deployment method and performance evaluation of gas sensor network based on field experiment, *Journal of Ambient Intelligence and Humanized Computing*, 12 (2021), 729–744.

[18] Qian, J. Y., *et al*., A numerical study of hydrogen leakage and diffusion in a hydrogen refueling station, *International Journal of Hydrogen Energy*, 45 (2020), 28, 14428–14439.

[19] Bellegoni, M., *et al*., Optimization of gas detectors placement in complex industrial layouts based on CFD simulations, *Journal of Loss Prevention in the Process Industries*, 80 (2022), 104859.

[20] Sklavounos, S., Rigas, F., Fuel gas dispersion under cryogenic release conditions, *Energy & Fuels*, 19 (2005), 6, 2535–2544.

[21] Dong, J. K., *et al*., Impact analysis of multi-sensor layout on the source term estimation of hazardous gas leakage, *Journal of Loss Prevention in the Process Industries*, 73 (2021), 104579.

[22] Dong, J. K., *et al*., Optimization of sensor deployment sequences for hazardous gas leakage monitoring and source term estimation, *Chinese Journal of Chemical Engineering*, 56 (2023), 169–179.

[23] Tanaka, T., et al., Experimental study on hydrogen explosions in a full-scale hydrogen filling station model, *International Journal of Hydrogen Energy*, 32(13) (2007), 2162–2170. https://doi.org/10.1016/j.ijhydene.2007.04.019

[24] Shirvill, L. C., et al., Safety studies on high-pressure hydrogen vehicle refueling stations: Releases into a simulated high-pressure dispensing area, *International Journal of Hydrogen Energy*, 37(8) (2012), 6949–6964. https://doi.org/10.1016/j.ijhydene.2012.01.030

[25] Kikukawa, S., Consequence analysis and safety verification of hydrogen fueling stations using CFD simulation, *International Journal of Hydrogen Energy*, 33(4) (2008), 1425–1434.

https://doi.org/10.1016/j.ijhydene.2007.11.027

[26] Kim, E., et al., Simulation of hydrogen leak and explosion for the safety design of hydrogen fueling station in Korea, *International Journal of Hydrogen Energy,* 38(3) (2013), 1737–1743. https://doi.org/10.1016/j.ijhydene.2012.08.079

[27] Idris, A. M., et al., A fuzzy multi-objective optimization model of risk-based gas detector placement methodology for explosion protection in oil and gas facilities, *Process Safety and Environmental Protection,* 161 (2022), 571–582. https://doi.org/10.1016/j.psep.2022.03.001

[28] Zhang, Y., et al., Progress and prospects of research on hydrogen sensors, *Chinese Science Bulletin,* 68(Z1) (2023), 204–219.

[29] Gao, Y., et al., Effects of leakage location and ventilation condition on hydrogen leakage during shipping of fuel cell vehicles, *International Journal of Hydrogen Energy,* 54 (2024), 1532–1543. https://doi.org/10.1016/j.ijhydene.2023.12.095

[30] Pu, L., et al., Numerical investigation on the difference of dispersion behavior between cryogenic liquid hydrogen and methane, *International Journal of Hydrogen Energy,* 44(39) (2019), 22368–22379. https://doi.org/10.1016/j.ijhydene.2019.05.219

Submitted: 17.02.2025
Revised: 24.03.2025
Accepted: 31.03.2025